Is correction for metallic artefacts mandatory in cardiac SPECT/CT imaging in the presence of pacemaker and implantable cardioverter defibrillator leads?

Original Article

Zahra Etemadi[1,2,3], Pardis Ghafarian[4,5], Ahmad Bitarafan-Rajabi[6], Hadi Malek[6], Arman Rahmim[7,8], Mohammad Reza Ay[2,3]

[1]Nuclear Medicine and Molecular Imaging Research Center, Namazi Teaching Hospital, Shiraz University of Medical Sciences, Shiraz, Iran
[2]Research Center for Molecular and Cellular Imaging, Tehran University of Medical Sciences, Tehran, Iran
[3]Department of Medical Physics and Biomedical Engineering, Tehran University of Medical Sciences, Tehran, Iran
[4]Chronic Respiratory Diseases Research Center, National Research Institute of Tuberculosis and Lung Diseases, Shahid Beheshti University of Medical Sciences, Tehran, Iran
[5]PET/CT and Cyclotron Center, Masih Daneshvari Hospital, Shahid Beheshti University of Medical Sciences, Tehran, Iran
[6]Cardiovascular Interventional Research Center, Department of Nuclear Medicine, Rajaei Cardiovascular, Medical, and Research Center, Iran University of Medical Sciences,Tehran, Iran
[7]Department of Radiology, Johns Hopkins University, Baltimore, Maryland, USA
[8]Department of Electrical and Computer Engineering, Johns Hopkins University, Baltimore, Maryland, USA

(Received 25 June 2017, Revised 5 August 2017, Accepted 11 August 2017)

ABSTRACT

Introduction: Metallic artifacts due to pacemaker/ implantable cardioverter defibrillator (ICD) leads in CT images can produce artifactual uptake in cardiac SPECT/CT images. The aim of this study was to determine the influence of the metallic artifacts due to pacemaker and ICD leads on myocardial SPECT/CT imaging.

Methods: The study included 9 patients who underwent myocardial perfusion imaging (MPI). A cardiac phantom with an inserted solid defect was used. The SPECT images were corrected for attenuation using both artifactual CT and CT corrected using metal artifact reduction (MAR). VOI-based analysis was performed in artifactual regions.

Results: In phantom studies, mean-of-relative-difference in white-region, between artifact-free attenuation-map without/with MAR were changed from 9.2 and 2.1 to 3.7 and 1.2 for ICD and pacemaker lead, respectively. However, these values for typical patient were 9.7±7.0 and 3.8±2.4 for ICD and pacemaker leads respectively, in white-region. MAR effectively reduces the artifacts in white-regions while this reduction is not significant in black-regions.

Conclusion: Following application of MAR, visual and quantification analyses revealed that while quality of CT images were significantly improved, the improvements in the SPECT/CT images were not as pronounced or significant. Therefore cardiac SPECT images corrected for attenuation using CT in the presence of metallic-leads can be interpreted without correction for metal artefacts.

Key words: Cardiac SPECT/CT; Metal artifact reduction; Virtual sonogram; Pacemaker; ICD

Iran J Nucl Med 2018;26(1):35-46
Published: January, 2018
http://irjnm.tums.ac.ir

Corresponding author: Dr. Pardis Ghafarian, Chronic Respiratory Diseases Research Center, National Research Institute of Tuberculosis and Lung Diseases (NRITLD), Shahid Beheshti University of Medical Sciences, Tehran, Iran.
E-mail: pardis.ghafarian@sbmu.ac.ir

INTRODUCTION

Evaluation of myocardial perfusion (MP) by SPECT imaging has become an important non-invasive method for diagnosis of coronary artery disease (CAD), therapy planning, and risk stratification [1]. Some quantification errors in myocardial perfusion in SPECT imaging can by induced by the effect of attenuation [2]. Multiple attempts [3] have been made to compensate for attenuation of the chest region in SPECT imaging, including implementation of CT-based attenuation correction (CTAC) [3]. Since introduction of cardiac SPECT/CT scanning in the clinic, diagnostic accuracy of myocardial perfusion (MP) by SPECT images has been improved [4, 5] but in addition to localization improvement [6], additional artifacts might be produced on the SPECT images [5]. The strong photoelectric absorption of X-rays due to the presence of highly attenuating objects such as metallic implants can exhibit white and black streak artifact in CT images [7]. Subsequently, incorrect Hounsfield units are transferred into the estimated attenuation map (μ-map), leading to errors in qualitative as well as quantitative analysis of radiotracer uptake in attenuation corrected SPECT images [7-11].

Different types of pacemaker and ICD leads are used for atria and ventricles, depending on the nature of the rhythm disruption in the patients [12]. DiFilippo, et al. [7] and Ghafarian et al. [12] determined the magnitude of the artifacts arising from metallic pacemaker and ICD leads in cardiac PET/CT imaging. They concluded that ICD-induced artifacts can degrade the quantitative accuracy of cardiac PET images in the CTAC procedure. It is worth noting that the density [12] and size [13] of metallic leads are important factors in induction of metallic artifacts.

Multiple algorithms have been proposed for metal artifact reduction (MAR) [14-16]. Generally, these algorithms are classified into two main categories: sinogram-based [17-20] and image-based [10, 21, 22] approaches. Lewitt et al. [23] introduced the first sinogram-based correction for MAR method using interpolation of missing data. The main idea of this method was to find the location of the missed bins in the affected projections by the metallic object in the raw CT data, and to replace them with reasonable values using a polynomial function. This method had a main drawback being the manipulation of a large portions of the CT raw data sets. As a framework to tackle this challenge, Abdoli et al. [20] introduced an effective concept of a virtual sinogram. In this approach, a virtual sinogram was produced by forward projecting the reconstructed CT, and a spline function was applied for estimating the missed projection bins.

The present work studies, for the first time, application of correction for metallic artifacts arising from the presence of ICD and pacemaker, in CTAC of myocardial SPECT data using the virtual sinogram method. We aimed to determine the influence of metallic artifacts due to the pacemaker and ICD leads on CT images, μ-maps, and MP images produced from SPECT data, using phantom as well as clinical studies. Furthermore, the impact of using virtual sinogram-based MAR method on CT data, μ-maps, and uptake value of myocardial wall in SPECT/CT images were investigated.

METHODS

SPECT/CT scanner

Cardiac SPECT/CT images were acquired by Symbia T2 SPECT/CT scanner (Siemens Medical Solutions, USA). The Symbia T2 SPECT was equipped with a pair of low-energy high-resolution parallel-hole collimators that use a proprietary design that provides uniform septa wall thickness. NaI(Tl) crystals are used in the detector of the SPECT scanner. The CT components are limited to two slices per rotation with 1344 channels per row.

Metallic implants

The influence of metallic artifacts on the SPECT/CT images of the cardiac phantom was assessed using a Sloex SR 60 pacemaker lead and a Kentrox RV 75 ICD lead (Biotronic, Berlin, Germany). The tip and ring of pacemaker and ICD electrodes are made of a Platinum/Iridium alloy. ICD lead also consists of defibrillation electrodes in the shock coils with 2.9 mm in diameter and 50 mm long that are made of Platinum/Iridium alloy.

Phantom study

A cardiac phantom (Cardiac Insert™, model ECT/CAR/I) was used in this study having a myocardium volume of 110 ml and a ventricle volume of 60 ml (Figure 1a). Solid defect insert 60° × 2 cm, with 5 mm wall thickness was placed to the outer of the ventricle volume for simulating left ventricular cold abnormalities. The myocardium wall was filled with a mixture of water and 73 MBq of ^{99m}TC-sestamibi (MIBI) according to routine clinical protocol. The cardiac ventricle was filled with water only. The pacemaker and ICD leads were attached separately to the outer side of the myocardium wall to generate metal artifact. The cardiac phantom with the attached leads was inserted in a cylindrical water phantom to produce attenuation medium (Figure 1b). To evaluate the effect of MAR algorithm, the phantom study was considered in two steps, with and without attached leads. It should be clear that the leads were put in parallel to the axial field-of-view (FOV) of the scanner, and the routine clinical protocol was used for data acquisition and reconstruction.

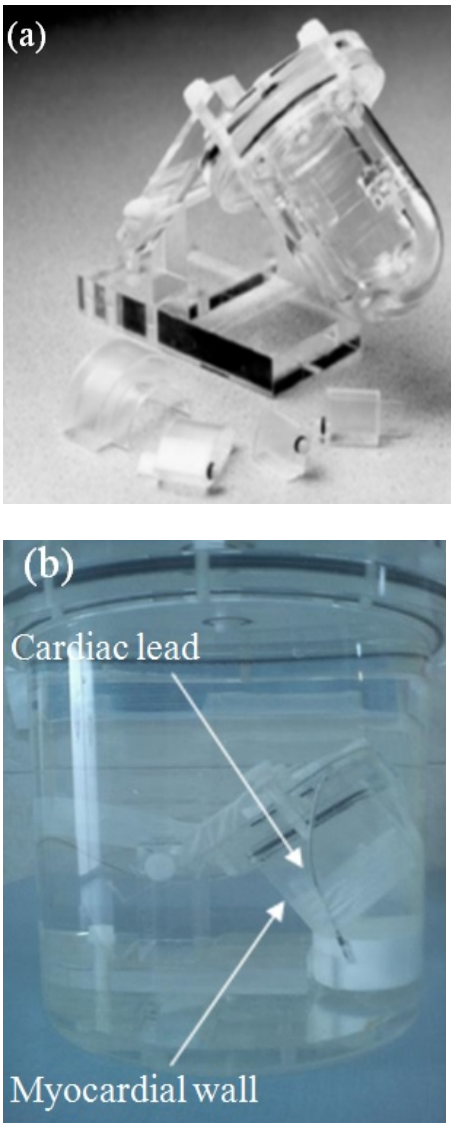

Fig 1. (a): The cardiac phantom (Cardiac Insert™, Model ECT/CAR/I) used in this study. (b): the attached ICD lead to cardiac phantom inside a cylindrical water phantom.

Clinical studies

In this study, we assessed 4 patients with pacemaker and 5 patients with ICD leads, who underwent MP imaging. The patients were injected with 740 MBq of ^{99m}Tc-Sestamibi, and after ~45 minutes they were scanned in the supine position with arms behind the head. The two scanner heads were set to an angle of 90°. A step-and-shoot SPECT acquisition (total of 32 projection views) was performed over 180°, from the right anterior oblique 45° to left posterior oblique 45° with a reconstruction matrix size of 64×64, zoom factor of 1.45, 30 second acquisition time per view, and 15% energy window set at 140 keV. Then, a 17-second CT acquisition was performed for attenuation correction (AC) in the chest area using a reconstruction matrix size of 512×512, slice thickness of 5 mm, tube voltage of 130 kV, and effective tube current of 17 mAs.

Image reconstruction

For evaluation of metallic artifact on SPECT/CT images, the SPECT images were reconstructed two times with and without MAR algorithm. A MAR algorithm with the concept of virtual sonogram [20], proposed to overcome the main problems (the large size of the CT raw data in implementing sinogram-based method), was used in this study (Figure 2). The method begins with forward projecting the reconstructed CT, considering the fan-beam geometry and projection parameters similar to the actual ones used in the CT scanner. The next step is the detection of the projection data affected by the metallic objects in the sinogram domain which was performed by forward projection the metal-only image. The metal-only image was generated by segmentation of the reconstructed CT image using simple thresholding, knowing that the metallic objects had CT numbers considerably higher than the other tissues. In the sinogram corresponding to the metallic objects, projection bins related to the unaffected pixels by the metallic objects, were set to zero. Subsequently, these projection bins in the artefactual sinogram were replaced by appropriate values using the spline interpolation method. Therefore, the corrected sinogram was back projected to obtain a reconstructed CT image with reduced metal-artifacts. Both forward and backward projections were performed by the same fan-beam geometry and parameters. The corrected CT image had the same size as the artefactual CT image. The attenuation corrected SPECT images with and without MAR were reconstructed using iterative reconstruction (ordered-subset expectation maximization, OSEM) with 6 iterations and 8 subsets.

Assessment strategy

Quantitative and qualitative analyses were performed for evaluation of the virtual sinogram-based MAR method in order to metallic artifact reduction arising of ICD and pacemaker leads in both cardiac phantom and clinical data. The analyses were performed in CT images, μ-maps and SPECT images. Various volume-of-interest (VOIs) were delineated in CT images and μ-maps, near and far from white and black artifacts. VOI analysis was also considered in individual myocardial segment of left ventricle in SPECT images. In the phantom study, white, black and unaffected regions were determined by comparison of the VOI value in the reference image (original artifact-free images) and artifactual CT images.

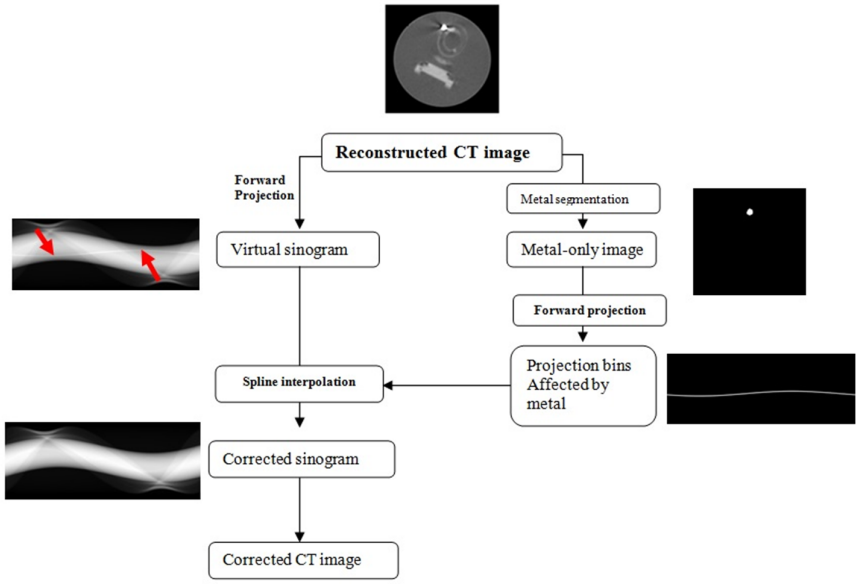

Fig 2. Flowchart of the virtual sinogram-based MAR algorithm used in this study.

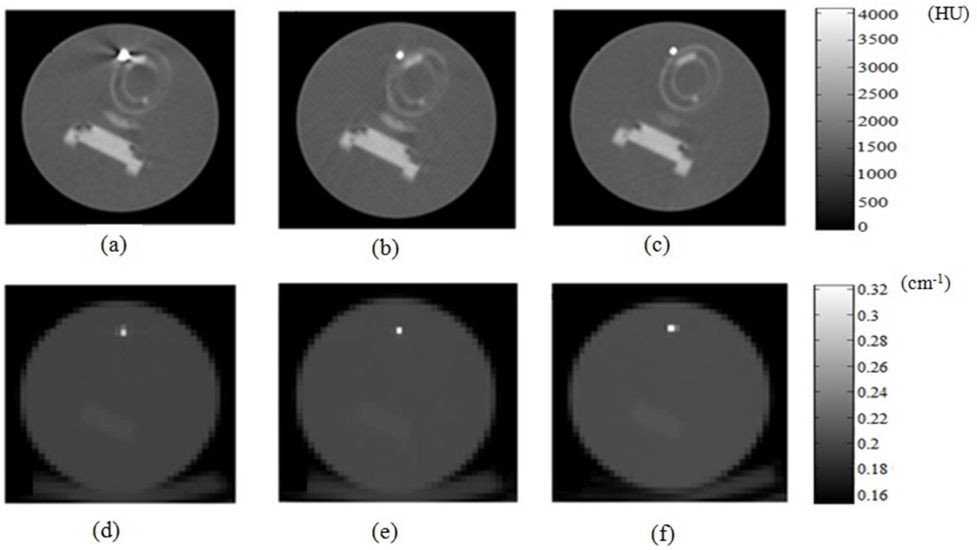

Fig 3. Transverce slice of cardiac phantom with ICD lead, (a): CT image without MAR,(b): CT image with MAR, (c): artefact free CT image with ICD lead,(d): generated μ-map without MAR,(e): generated μ-map with MAR,(f): generated μ-map of artefact free CT image.

The artifact-free CT image was acquired by segmenting the metal from the artifactual CT image and then superimposing the metal to metal-free CT image. Artifact-free images with ICD and pacemaker leads were compared with images reconstructed without and with the MAR algorithm, by box and whisker plots. Mean relative differences between actual and measured uptake values in SPECT images, corrected for attenuation without and with MAR, were calculated in the phantom study. The mean relative difference between the defined VOIs on the CT image (μ-map) and SPECT images without and with MAR were calculated in clinical data. SPECT images were reoriented along the short axis, horizontal and vertical long axis views. 17-segment bull's eye view were also utilized as generated by the QPS analysis program [24] for better interpretation.

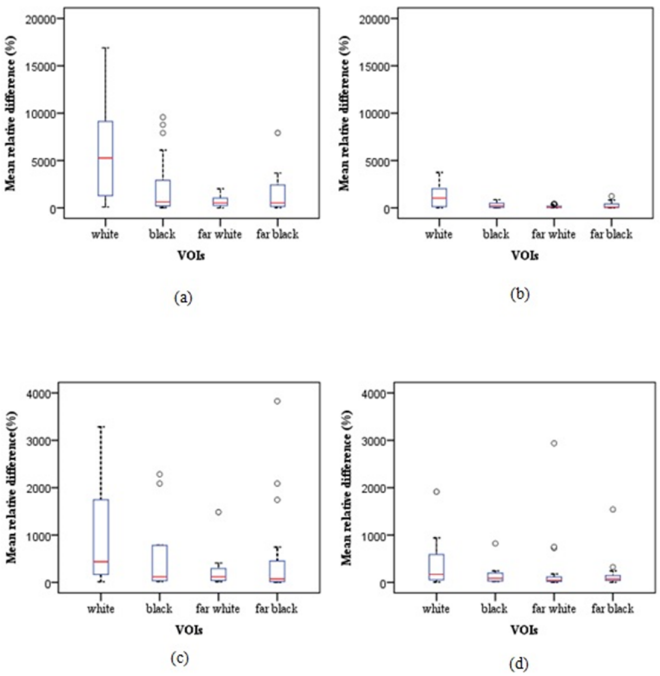

Fig 4. Distribution of relative difference using Box and Whisker plots are shown between artefact-free CT images and (a): CT image with ICD lead without MAR, (b): CT image with ICD lead with MAR,(c): CT image with pacemaker lead without MAR, (d): CT image with pacemaker lead with MAR.

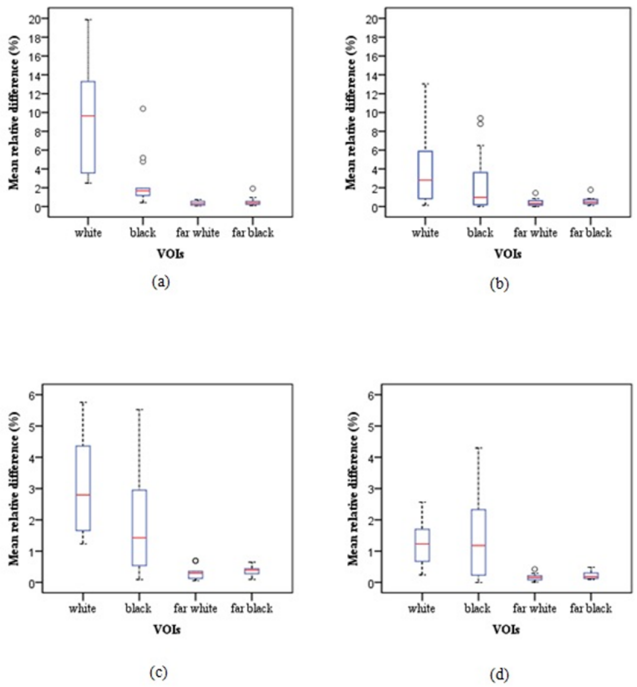

Fig 5. Distribution of relative difference using Box and Whisker plots are shown between artefact-free µ-map and (a): µ-map with ICD lead without MAR, (b): µ-map with ICD lead with MAR,(c): µ-map with pacemaker lead without MAR, (d); µ-map with pacemaker lead with MAR.

Visual analysis was performed by two expert NM physicians by reviewing the AC SPECT images before and after performing MAR algorithm in the CT images. In addition, coronary angiography (CA) was considered as a gold standard for evaluating the influence of the MAR algorithm in metal artifact reduction in SPECT images for five patients with CA reports.

Statistical analysis

The two-sided paired t-test analysis was used to compare images reconstructed with and without MAR algorithm. Statistical analysis was considered using SPSS software (SPSS, version 22.0, Armonk, NY). P-values less than 0.05 were assessed as statistically significant.

RESULTS

Figure 3 shows the CT images and μ-maps of the cardiac phantom with ICD lead, before and after applying MAR algorithm in association with artifact-free CT image and corresponding μ-map. The intensity of metal artifact reduction is more evidence in CT images versus to μ-map after applying MAR algorithm. Distribution of relative difference between artifact-free CT image (μ-map) and CT image without and with MAR (μ-map) algorithm in all regions, including white, black, far white and far black, are illustrated when ICD and pacemaker leads are utilized in cardiac phantom (Figures 4 and 5). In general, significant overestimation of CT number was observed for ICD lead versus to pacemaker lead.

The overestimation of CT numbers in white, black, far white and far black reduced significantly when MAR algorithm was applied for ICD lead (Table 1). However, the intensity of artifact reduction is less pronounced in μ-maps of ICD, where significant effect is only observed for white region (from 9.2 to 3.7, $p<0.001$). However, more effect of MAR algorithm effectiveness is observed in white region of pacemaker lead in CT image in comparison with black area artifacts (from 1194.5 to 598.3, $p=0.018$) and μ-map (from 2.1 to 1.2, $p=0.097$). The SPECT images of cardiac phantom with defect in the anterior septum wall, with attached ICD lead, in addition to bull's eye view are illustrated in Figure 6. It is interesting that visual analysis in short axis, horizontal and vertical long axes did not shown significant variation before and after applying MAR algorithm. However, MAR algorithm can alter some artefactual variation in all regions of bull's eye views.

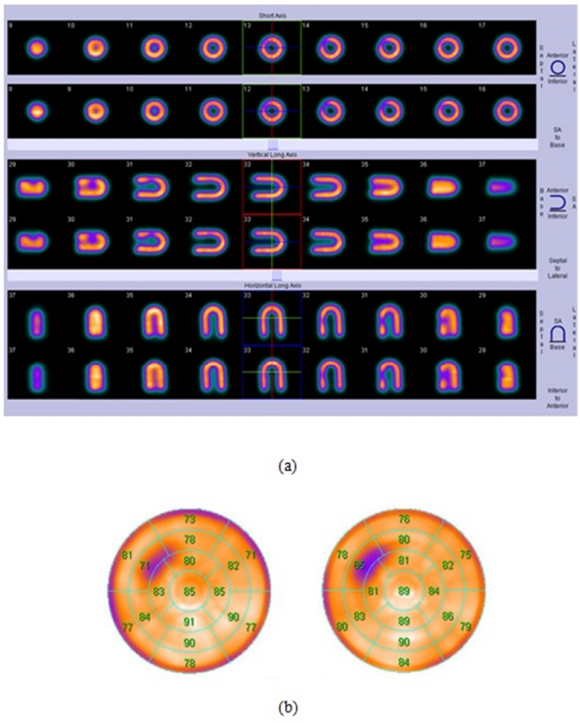

Fig 6. (a): short axis, vertical and horizontal long axis of SPECT image of cardiac phantom corrected for attenuation with anterior septum wall defect for the ICD lead without MAR (top row) and with MAR (bottom row), (b): Bull's eye view of SPECT images corrected for attenuation without MAR (left) and with MAR (right).

Table1: Mean of relative differences in VOIs drawn between free-artefact and artefactual CT and μ-map images reconstructed without/with MAR in white and black regions, near and far from metal's location, in phantom study.

	ICD						Pacemaker					
	No MAR		MAR		p-value		No MAR		MAR		p-value	
	CT	μ-map	CT	μ-map	CT	μ-map	CT	μ-map	CT	μ-map	CT	μ-map
White	7137.3 ±352.1	9.2 ±0.441	3585.0 ±147.4	3.7 ±0.169	0.014	<0.001	1194.5 ±56.4	3.0 ±0.178	598.3 ±28.4	1.2 ±0.066	0.018	0.011
Black	2186.6 ±87.1	2.6 ±0.100	302.1 ±16.2	2.5 ±0.118	<0.001	0.816	619.0 ±28.2	1.9 ±0.087	176.7 ±5.9	1.5 ±0.077	0.127	0.477
Far white	694.7 ±30.6	0.3 ±0.014	112.0 ±6.7	0.4 ±0.013	<0.001	0.518	215.8 ±11.3	0.3 ±0.016	230.2 ±11.6	0.1 ±0.006	0.903	0.063
Far black	2085.0 ±91.3	0.4 ±0.021	250.7 ±12.6	0.5 ±0.027	0.025	0.364	534.0 ±26.1	0.3 ±0.020	172.3 ±8.1	0.2 ±0.015	0.038	0.344

Table 2: Mean of relative difference in uptake value between absolute activity and the activity extracted from images reconstructed without CTAC (SPECT only), CTAC without MAR (SPECT/CT without MAR) and CTAC with MAR (SPECT/CT with MAR) in both white and black regions near ICD and pacemaker leads.

	SPECT		SPECT/CT without MAR		SPECT/CT with MAR	
	Overestimated (White region)	**Underestimated** (Black region)	**Overestimated** (White region)	**Underestimated** (Black region)	**Overestimated** (White region)	**Underestimated** (Black region)
ICD	23.1±3.5 (p<0.001)	21.7±2.9 (p<0.001)	-15.6±3.4 (p<0.05)	11.1±1.6 (p=0.04)	-9.4±4.9 (p<0.05)	9.6±3.7 (p=0.085)
Pacemaker	22.8±1.7 (p<0.001)	20.9±1.7 (p<0.001)	-9.8±1.5 (p<0.05)	6.5±3.3 (p=0.126)	-5.1±1.4 (p=0.232)	5.1±2.7 (p=0.145)

The mean of relative differences according to VOI analysis for both SPECT and CTAC SPECT (SPECT/CT) images of cardiac phantom are shown in Table 2. The comparison was performed for both white and black regions near ICD and pacemaker leads. The actual activity was compared with measured activity in phantom before and after applying MAR algorithm. It is noticeable that the MAR algorithm can result in greater artifact reduction in white regions versus black regions for both ICD and pacemaker leads. For ICD lead patients, mean of relative differences in SPECT/CT images corrected for attenuation varied from -15.6±3.4 and 11.1±1.6 to -9.4±4.9 and 9.6±3.7 for white and black regions, respectively. By comparison, for pacemaker lead patients, mean of relative differences varied from -9.6±1.5 and 6.5±3.3 to -5.1±1.4 and 5.1±2.7 for black and white regions, respectively regions.

Figure 7 show CT images, μ-maps, and difference images of a transverse slice of a typical patient with ICD leads obtained with and without MAR. The impact of MAR algorithm is seen in difference images of both CT images and μ-maps.

Table 3 summarized the mean of relative differences between μ-map generated without and with MAR algorithm, in the white, black, and unaffected regions in all patients with ICD and pacemaker leads. It is clear that MAR algorithm introduces more impact in ICD lead versus to pacemaker due to high atomic number effect and is more effective for white region with compared to black region.

SPECT images of typical patient with ICD and pacemaker leads in addition to bull's-eye views are shown in Figures 8 and 9, respectively. It is noted that, although some variations was observed in all regions in bull's eye views after applying MAR algorithm, visual assessment in standard cardiac axes in association with bull's eye views did not lead to significant difference in clinical interpretation. Furthermore, in the case of patients with CA report, qualitative assessment demonstrated no significant difference between both cardiac SPECT results without/with MAR and their CA reports. Mean relative differences between uptake values in SPECT images corrected for attenuation without and with MAR algorithm according to 17 segment bull's eye view analysis for all patients in this study are shown in Table 4. No significant differences for SPECT images without vs. with MAR algorithm, when pacemaker lead was utilized, are seen.

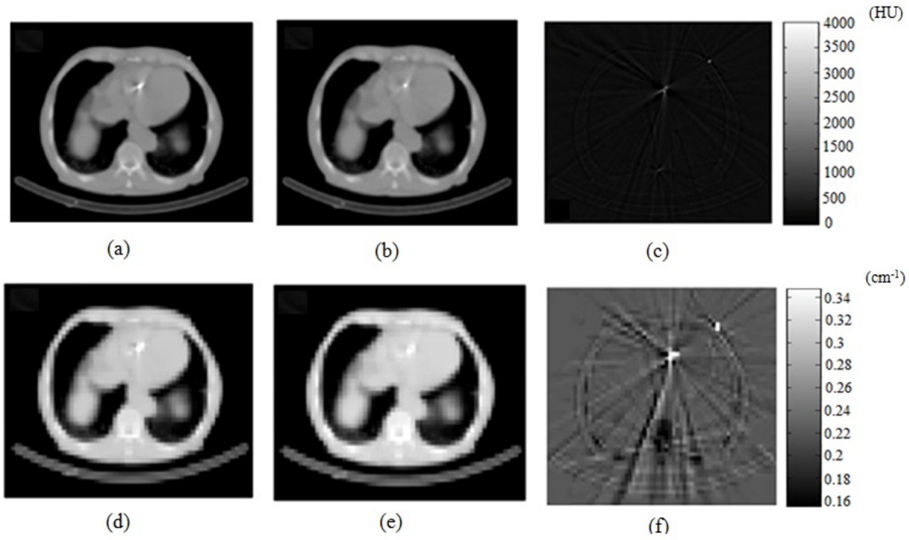

Fig 7. Typical transverse slice of patient with ICD lead, (a): CT image reconstructed without MAR, (b): CT image reconstructed with MAR, (c): difference image between CT images, (d): μ-map generated without MAR,(e): μ-map generated with MAR, (f): difference image between μ-maps.

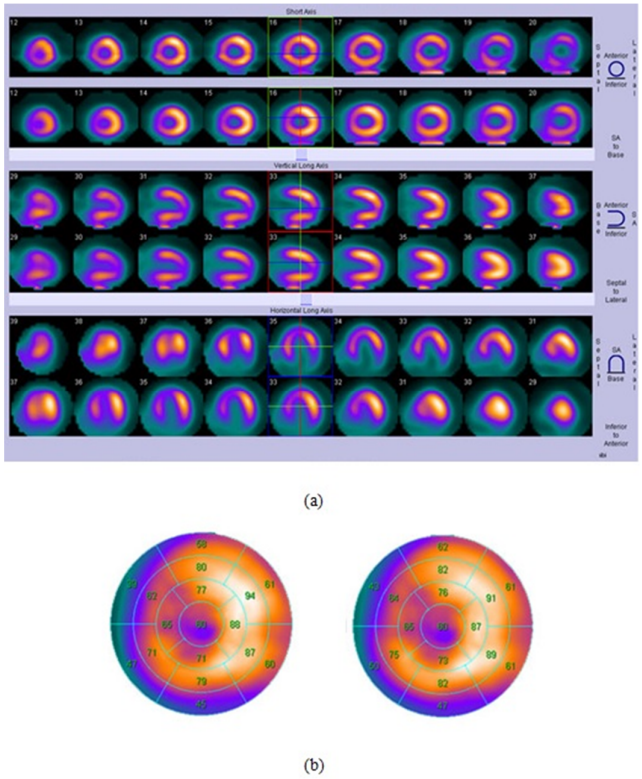

Fig 8. (a): short axis, vertical and horizontal long axis of SPECT image of a typical patient with ICD lead corrected for attenuation without MAR (top row) and with MAR (botom row) (b): Bull's eye view of SPECT images corrected for attenuation without MAR (left) and with MAR (right).

Table 3: Mean of relative differences in linear attenuation coefficients (μ-map) for all patients included in this study between μ-maps generated without and with MAR in white, black and unaffected regions (patients 1–5 with ICD leads, patients 6–9 with pacemaker leads).

Patient study	White Region	Black Region	Unaffected Region
1	5.4 ± 2.6 (p<0.05)	-3.7 ± 3.2 (p<0.05)	0.4 ± 0.3 (p=0.739)
2	5.7 ± 4.8 (p=0.131)	-3.3 ± 4.2 (p=0.085)	0.4 ± 0.3 (p=0.155)
3	9.7 ± 7.0 (p<0.001)	-5.2 ± 4.3 (p=0.128)	1.3 ± 1.8 (p=0.782)
4	6.2 ± 5.6 (p<0.001)	-7.0 ± 7.0 (p<0.005)	1.4 ± 1.4 (p=0.712)
5	4.0 ± 5.0 (p=0.942)	-4.1 ± 4.0 (p=0.828)	0.2 ± 0.1 (p=0.376)
6	3.8 ± 2.4 (p<0.05)	-0.92 ± 1.0 (p=0.324)	0.5 ± 0.4 (p=0.689)
7	2.7 ± 2.6 (p=0.157)	-1.8 ± 1.8 (p=0.074)	0.5 ± 0.2 (p=0.383)
8	2.4 ± 2.0 (p=0.108)	-3.1 ± 2.3 (p<0.05)	0.6 ± 0.6 (p=0.762)
9	0.8 ± 0.7 (p=0.180)	-1.6 ± 1.5 (p<0.05)	0.2 ±0.1 (p<0.05)

Table 4: Mean of relative difference in uptake value of SPECT images corrected for attenuation without and with MAR algorithm for all patients included in this study.

Myocardial segments	ICD lead	Pacemaker lead
Basal anterior	12.1 ± 5.3 (p=0.339)	4.6 ± 3.2 (p=0.942)
Basal anterior septum	12.3 ± 2.7 (p=0.691)	5.4 ± 6.3 (p=0.908)
Basal inferior septum	12.2 ± 4.7 (p=0.757)	7.2 ± 7.0 (p=0.906)
Basal inferior	9.2 ± 2.2 (p=0.701)	4.4 ± 3.6 (p=0.971)
Basal inferior lateral	10.6 ± 5.3 (p=0.677)	6.7 ± 4.8 (p=0.929)
Basal anterior lateral	8.5 ± 3.2 (p=0.622)	6.0 ± 4.6 (p=0.939)
Middle anterior	13.3 ± 6.4 (p=0.404)	5.7 ± 6.8 (p=0.825)
Middle anterior septum	14.6 ± 7.1 (p=0.532)	5.8 ± 5.7 (p=0.949)
Middle inferior septum	13.6 ± 7.1 (p=0.448)	5.5 ± 5.6 (p=0.991)
Middle inferior	13.9 ± 5.2 (p=0.170)	3.6 ± 2.3 (p=0.883)
Middle inferior lateral	11.5 ± 4.2 (p=0.471)	4.0 ± 2.1 (p=0.907)
Middle anterior lateral	14.9 ± 5.3 (p=0.121)	4.1 ± 2.7 (p=0.841)
Apical anterior	16.0 ± 9.7 (p=0.424)	8.0 ± 8.1 (p=0.960)
Apical septum	14.6 ± 9.0 (p=0.535)	3.4 ± 3.2 (p=0.999)
Apical inferior	15.5 ± 7.2 (p=0.220)	3.8 ± 4.5 (p=0.939)
Apical lateral	17.3 ± 9.7 (p=0.105)	5.6 ± 4.0 (p=0.953)
Apex	10.1 ± 6.7 (p=0.560)	5.3 ± 4.3 (p=0.900)

DISCUSSION

In our previous work, we developed virtual sinogram-based method for metal artifact reduction (MAR) for dental implant artifact in CTAC of the PET data [20]. In the current study, the impact of using this method was evaluated for reduction of streak artifacts arising of ICD and pacemaker leads in CT images, μ-maps and cardiac SPECT/CT projections, corrected for attenuation, using CT images. White and black artifact can introduce some overestimation and underestimation of uptake value in PET/CT images [12, 15, 25-27]. Nahmias et al. [28] demonstrated that the MAR method that they used had no effect on the interpretation of the PET images in CTAC studies of oral as well as head and neck cancer. Suzuki et al. [9] clarified the influence of cardiac implants on CTAC of the SPECT data. They observed overestimation due to cardiac leads, but mentioned that CTAC can be effective to correct attenuation of the inferior and anteroseptal walls for SPECT images. To the best of our knowledge, the effect of streak artifact on the uptake value in SPECT/CT images using virtual sinogram-based method had not been previously evaluated , while, the influence of metallic artifacts and the different MAR methods for reducing these artifacts in CT images [29] and PET/CT images [10, 16, 21, 28, 30, 31] were investigated.

In our study, we showed that MAR can be effective in reduction of metal artefacts on the CT images and to some extent in μ-maps.

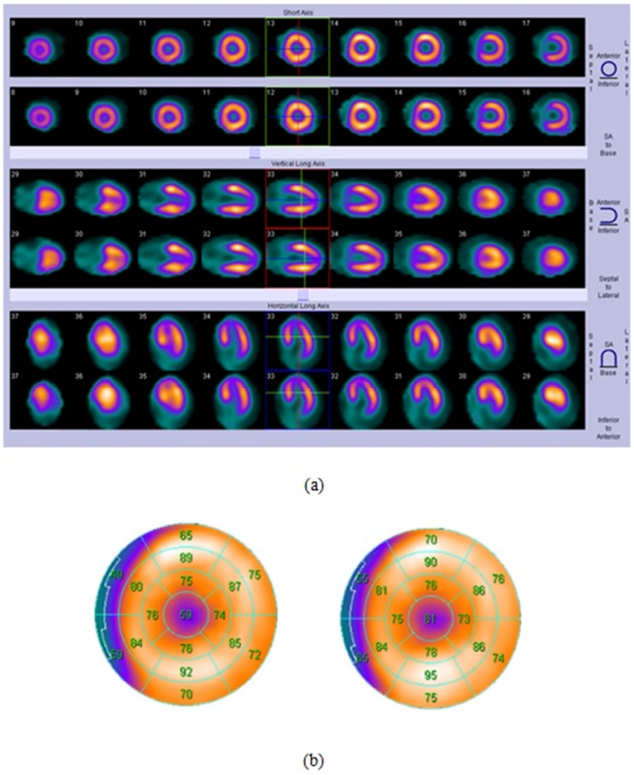

Fig 9. (a): short axis, vertical and horizontal long axis of SPECT image of a typical patient with pacemaker lead corrected for attenuation without MAR (top row) and with MAR (botom row) (b): Bull's eye view of SPECT images corrected for attenuation without MAR (left) and with MAR (right).

Metallic artifact can be visible on μ-maps with less intensity because of smoothing (as a result of poor spatial resolution of SPECT images - around 10-15 mm), as well as down sampling and energy mapping procedures. The effective result of MAR algorithm was seen in white artifact regions especially in the close distance of metal and were more effective for ICD leads as opposed to pacemaker leads. The maximum value for mean of relative difference for linear attenuation coefficient between images reconstructed without/with MAR was 9.7 ± 7.0 and 3.8 ± 2.4 for ICD and pacemaker leads in white region, respectively. While the maximum value for black regions were -7.0 ± 7.0 and -3.1 ± 2.3 for ICD and pacemaker leads, respectively.

We did not observe significantly different values for linear attenuation coefficient using without/with MAR for regions far from either metallic leads. In the SPECT/CT images, MAR method generated strong effects in white artifact regions especially in proximity to the metal, and it was more effective in ICD versus pacemaker leads. In PET/CT images, Ghafarian et al. [12] and DiFilippo et al. [7] showed that increased uptake values were more pronounced for ICD than pacemaker leads, which is in line with our findings in this study. The mean relative difference of uptake value with regard to the 17 segment bull's eye views in SPECT images without and with MAR algorithm revealed overestimation of uptake value for both ICD and pacemaker leads. The intensity of overestimation was less for pacemaker leads due to lower atomic number. Using MAR can be more effective in ICD leads for all segments of bull's eye view versus pacemaker leads. However, the overestimation of uptake value was not significant for all segments of myocardial bull's eye view when pacemaker lead were used. Although overestimation of uptake value was observed in SPECT/CT images, the clinical interpretation was not changed after applying MAR algorithm for the patients in our study. For patients with coronary angiography (3 with ICD and 2 with pacemaker), no significant differences were observed between cardiac SPECT reconstructed without or with MAR as compared to coronary angiographic findings. It should be noted that in the case of phantom and for patients without CA report, visual interpretation did not demonstrate a significant difference between the two attenuation-corrected SPECT images

(without/with MAR) as reoriented along standard cardiac axes. It is worth noting that different overestimation of uptake value was observed for different patients with ICD and pacemaker leads, that can be related to the location of ICD and pacemaker used, in patients included in this study. The same behavior was observed in the case of PET/CT [12].

CONCLUSION

In the present study, the impact of a virtual sinogram-based method for correction of metal artifacts arising from ICD and pacemaker leads was evaluated, in cardiac SPECT/CT imaging. Our study showed that the proposed metal-artifact reduction (MAR) algorithm is more effective in white regions artifacts versus black regions especially for ICD leads in CT images. However, this overall improvement was noticed to be less pronounced in SPECT/CT images reconstructed either from phantom or clinically obtained data. Overestimation of uptake value was more for ICD as opposed to pacemaker leads in all myocardial segments. However, the overall effect for the clinical interpretation of cardiac SPECT/CT images was not significant. It can therefore be argued that cardiac SPECT images based on CT reconstruction and attenuation correction, despite the presence of metallic leads, can comfortably be interpreted without the need for metallic artifacts compensation.

Acknowledgments

The authors would like to thank the staff of the Department of Nuclear Medicine, Shahid Rajae Hospital, for support. This work was supported by the Research Center for Molecular and Cellular Imaging, Tehran University of Medical Sciences, under grant No. 25938.

REFERENCES

1. Da Silva AJ, Tang HR, Wong KH, Wu MC, Dae MW, Hasegawa BH. Absolute quantification of regional myocardial uptake of 99mTc-sestamibi with SPECT: experimental validation in a porcine model. J Nucl Med. 2001 May;42(5):772-9.
2. Heller GV, Bateman TM, Johnson LL, Cullom SJ, Case JA, Galt JR, Garcia EV, Haddock K, Moutray KL, Poston C, Botvinick EH, Fish MB, Follansbee WP, Hayes S, Iskandrian AE, Mahmarian JJ, Vandecker W. Clinical value of attenuation correction in stress-only Tc-99m sestamibi SPECT imaging. J Nucl Cardiol. 2004 May-Jun;11(3):273-81.
3. Singh B, Bateman TM, Case JA, Heller G. Attenuation artifact, attenuation correction, and the future of myocardial perfusion SPECT. J Nucl Cardiol. 2007 Apr;14(2):153-64.
4. Germano G, Slomka PJ, Berman DS. Attenuation correction in cardiac SPECT: the boy who cried wolf? J Nucl Cardiol. 2007 Jan;14(1):25-35.
5. Bybel B, Brunken RC, DiFilippo FP, Neumann DR, Wu G, Cerqueira MD. SPECT/CT imaging: clinical utility of an emerging technology. Radiographics. 2008 Jul-Aug;28(4):1097-113.
6. Utsunomiya D, Tomiguchi S, Shiraishi S, Yamada K, Honda T, Kawanaka K, Kojima A, Awai K, Yamashita Y. Initial experience with X-ray CT based attenuation correction in myocardial perfusion SPECT imaging using a combined SPECT/CT system. Ann Nucl Med. 2005 Sep;19(6):485-9.
7. DiFilippo FP, Brunken RC. Do implanted pacemaker leads and ICD leads cause metal-related artifact in cardiac PET/CT? J Nucl Med. 2005 Mar;46(3):436-43.
8. Yamada S, Ueguchi T, Shimosegawa E, Fujino K, Shimazu T, Murase K, Hatazawa J. Feasibility of improved attenuation correction for SPECT reconstruction in the presence of dense materials using dual-energy virtual monochromatic CT: A phantom study. Open J Med Imaging. 2015 Dec;5(4):183-93.
9. Suzuki A, Koshida K, Matsubara K. Effects of pacemaker, implantable cardioverter-defibrillator, and left ventricular leads on CT-based attenuation correction. J Nucl Med Technol. 2014 Mar;42(1):37-41.
10. Mirzaei S, Guerchaft M, Bonnier C, Knoll P, Doat M, Braeutigam P. Use of segmented CT transmission map to avoid metal artifacts in PET images by a PET-CT device. BMC Nucl Med. 2005 Jun 14;5(1):3.
11. Amarasekera HW, Costa ML, Parsons N, Achten J, Griffin DR, Manktelow S, Williams NR. SPECT/CT bone imaging after hip resurfacing arthroplasty: is it feasible to use CT attenuation correction in the presence of metal implants? Nucl Med Commun. 2011 Apr;32(4):289-97.
12. Ghafarian P, Aghamiri SM, Ay MR, Rahmim A, Schindler TH, Ratib O, Zaidi H. Is metal artefact reduction mandatory in cardiac PET/CT imaging in the presence of pacemaker and implantable cardioverter defibrillator leads? Eur J Nucl Med Mol Imaging. 2011 Feb;38(2):252-62.
13. Ay MR, Zaidi H. Impact of X-ray tube settings and metallic leads on neurological PET imaging when using CT-based attenuation correction. Nucl Instrum Methods Phys Res A: Accelerators, Spectrometers, Detectors and Associated Equipment. 2007;571(1-2):411-4.
14. Mehranian A, Ay MR, Rahmim A, Zaidi H. 3D prior image constrained projection completion for X-ray CT metal artifact reduction. IEEE Trans Nucl Sci. 2013 Sep;60(5):3318-32.
15. Mehranian A, Ay M, Rahmim A, Zaidi H. Metal artifact reduction in CT-based attenuation correction of PET using sobolev sinogram restoration. IEEE Nucl Sci Symp Med Imaging Conf Rec. 2011 Oct;2936-42.
16. Abdoli M, Ay MR, Ahmadian A, Dierckx RA, Zaidi H. Reduction of dental filling metallic artifacts in CT-based attenuation correction of PET data using weighted virtual sinograms optimized by a genetic algorithm. Med Phys. 2010 Dec;37(12):6166-77.
17. Bazalova M, Beaulieu L, Palefsky S, Verhaegena F. Correction of CT artifacts and its influence on Monte Carlo dose calculations. Med Phys. 2007 Jun;34(6):2119-32.
18. Kalender WA, Hebel R, Ebersberger J. Reduction of CT artifacts caused by metallic implants. Radiology. 1987 Aug;164(2):576-7.
19. Mahnken AH, Raupach R, Wildberger JE, Jung B, Heussen N, Flohr TG, Günther RW, Schaller S. A new algorithm for metal artifact reduction in computed tomography: in vitro

and in vivo evaluation after total hip replacement. Invest Radiol. 2003 Dec;38(12):769-75.

20. Abdoli M, Ay MR, Ahmadian A, Zaidi H. A virtual sinogram method to reduce dental metallic implant artefacts in computed tomography-based attenuation correction for PET. Nucl Med Commun. 2010 Jan;31(1):22-31.

21. Hamill JJ, Brunken RC, Bybel B, DiFilippo FP, Faul DD. A knowledge-based method for reducing attenuation artefacts caused by cardiac appliances in myocardial PET/CT. Phys Med Biol. 2006 Jun 7;51(11):2901-18.

22. Kennedy JA, Israel O, Frenkel A, Bar-Shalom R, Azhari H. The reduction of artifacts due to metal hip implants in CT-attenuation corrected PET images from hybrid PET/CT scanners. Med Biol Eng Comput. 2007 Jun;45(6):553-62.

23. Lewitt R, Bates R. Image-reconstruction from projections. 3. Projection completion methods (theory). Optik. 1978 April;50:189-204.

24. Sharir T, Germano G, Waechter PB, Kavanagh PB, Areeda JS, Gerlach J, Kang X, Lewin HC, Berman DS. A new algorithm for the quantitation of myocardial perfusion SPECT. II: validation and diagnostic yield. J Nucl Med. 2000 Apr;41(4):720-7.

25. Harnish R, Prevrhal S, Alavi A, Zaidi H, Lang TF. The effect of metal artefact reduction on CT-based attenuation correction for PET imaging in the vicinity of metallic hip implants: a phantom study. Ann Nucl Med. 2014 Jul;28(6):540-50.

26. Abdoli M, de Jong JR, Pruim J, Dierckx RA, Zaidi H. Reduction of artefacts caused by hip implants in CT-based attenuation-corrected PET images using 2-D interpolation of a virtual sinogram on an irregular grid. Eur J Nucl Med Mol Imaging. 2011 Dec;38(12):2257-68.

27. Ay MR, Mehranian A, Abdoli M, Ghafarian P, Zaidi H. Qualitative and quantitative assessment of metal artifacts arising from implantable cardiac pacing devices in oncological PET/CT studies: a phantom study. Mol Imaging Biol. 2011 Dec;13(6):1077-87.

28. Nahmias C, Lemmens C, Faul D, Carlson E, Long M, Blodgett T, Nuyts J, Townsend D. Does reducing CT artifacts from dental implants influence the PET interpretation in PET/CT studies of oral cancer and head and neck cancer? J Nucl Med. 2008 Jul;49(7):1047-52.

29. Abdoli M. Evaluation strategies for metal artifact reduction approaches in CT: A literature survey. Front Biomed Technol. 2014;1(2):82-90.

30. Nuyts J, Stroobants S. Reduction of attenuation correction artifacts in PET-CT. IEEE Nucl Sci Symp Med Imaging Conf Rec. 2005 Oct; 5.

31. Kondo A, Hayakawa Y, Dong J, Honda A. Iterative correction applied to streak artifact reduction in an X-ray computed tomography image of the dento-alveolar region. Oral Radiol. 2010 Jun;26(1):61-5.